A multi-method field experiment to determine local groundwater flow in a glacier forefield

Florian Kobierska,[1,2]* Tobias Jonas,[1] Nena Griessinger,[1] Christian Hauck,[3] Stephan Huxol[4] and Stefano M. Bernasconi[2]

[1] *WSL Institute for Snow and Avalanche Research SLF, Davos, Switzerland*
[2] *Geological Institute, ETH Zurich, Sonnegstrasse 5, 8092 Zürich, Switzerland*
[3] *Department of Geosciences, University of Fribourg, Chemin du Musée 4, 1700 Fribourg, Switzerland*
[4] *EAWAG, Swiss Federal Institute of Aquatic Science and Technology, Duebendorf, Switzerland*

Abstract:

We implemented multiple independent field techniques to determine the direction and velocity of groundwater flow at a specific stream reach in a glacier forefield. Time-lapse experiments were conducted using two electrical resistivity tomography (ERT) lines installed in a cross pattern. A circular array of groundwater tubes was also installed to monitor groundwater flow via discrete salt injections. Both inter-borehole and ERT results confirmed this stream section as a losing reach and enabled quantification of the flow direction. Both techniques yielded advection velocities varying between 5.7 and 21.8 m/day. Estimates of groundwater flow direction and velocity indicated that groundwater infiltrates from the stream nearby and not from the adjacent lateral moraine. Groundwater age estimated from radon concentration measurements supported this hypothesis. Despite uncertainties inherent to each of the methods deployed, the combination of multiple field techniques allowed drawing consistent conclusions about local groundwater flow. We thus regard our multi-method approach as a reliable way to characterize the two-dimensional groundwater flow at sites where more invasive groundwater investigation techniques are difficult to carry out and local heterogeneities can make single measurements unreliable.

KEY WORDS mountain hydrology; groundwater flow; stream-groundwater interactions; ERT; tracer experiments; radon

INTRODUCTION

Mountain watersheds play an important role in the hydrological cycle. With receding glaciers, the evolution of melt water sources will impact groundwater storage. This could have consequences on winter base-flow, thereby modifying the flow regimes of rivers downstream and influencing irrigation, hydro-electrical and flood management decisions. In this paper, we investigate water exchanges between stream and riparian zone at a specific stream reach of an alpine glacier forefield.

Our field site is the Damma glacier forefield in central Switzerland (Bernasconi and BigLink consortium, 2011; Magnusson *et al*., 2012a, b; Kobierska *et al*., 2013) and is currently being studied as one of the Critical Zone Observatories of the SoilTrEC project (Soil Transformations in European Catchments, see Banwart *et al*., 2011). Magnusson *et al*. (2012a) simulated the propagation of daily stream stage fluctuations into the aquifer at four transects with a diffusion model. By considering the shortest distance to the groundwater tubes, the study focused on the lateral impact of stream stage fluctuations into the riparian zone. Hydraulic conductivities estimated with this modelling approach were compared with slug tests results. Such an approach, however, concentrated on the lateral groundwater stage variations, therefore dismissing the two-dimensional properties of the groundwater flow. In this paper, we aim to extend our understanding of stream-groundwater interactions in two dimensions. We focus on the estimation of hydraulic conductivities and groundwater flow directions at one particularly well-instrumented section of the forefield.

Groundwater and stream water interactions can be extremely difficult to determine. Moreover, in mountainous areas, classical groundwater characterization methods such as pumping tests (Kalbus *et al*., 2006) are impractical or impossible to carry out. The heterogeneity of hydraulic properties typically makes point-scale measurements too unreliable for the determination of average aquifer properties. To alleviate these issues, we chose to associate various field techniques. We used both invasive and non-invasive methods to monitor two-dimensional groundwater flow and

*Correspondence to: Florian Kobierska, WSL Institute for Snow and Avalanche Research SLF, Fluelastrasse 11, CH-7260 Davos Dorf, Switzerland. E-mail: kobierska@slf.ch

complement earlier hydraulic conductivity estimates. The invasive techniques were based on the installation of boreholes, which were used for groundwater stage monitoring, salt tracer experiments and radon concentration measurements. The non-invasive technique was electrical resistivity tomography (ERT), using lines that were specifically designed and constructed to be left on site for repeated autonomous measurements.

Time-lapse ERT monitoring has been increasingly used to monitor permafrost (Hauck, 2002; Hilbich *et al*., 2011; Scherler *et al*., 2012) and subsurface hydrological processes (Singha and Gorelick, 2005; Miller *et al*., 2008; Binley *et al*., 2010; Ward *et al*., 2010). ERT is often used to follow salt plumes, albeit in relatively controlled environments (i.e. Kemna *et al*., 2002; Garré *et al*., 2010). Literature on salt tracer experiments describes cross-borehole ERT as the method of choice for such studies (Perri *et al*., 2012). This approach was not feasible for this study as drilling many deep boreholes would have been extremely costly and logistically difficult at this particular field site.

The main objectives of this study are (1) to estimate local groundwater flow direction and velocity, (2) to increase confidence in those estimates by linking the results of different experimental methods and (3) to combine groundwater flow properties with residence times estimates in order to formulate a conceptual model of the two-dimensional groundwater flow at the site investigated. For these purposes, we conducted salt tracer experiment using time-lapse ERT, groundwater stage measurements, inter-borehole salt tracer tests and radon concentration surveys.

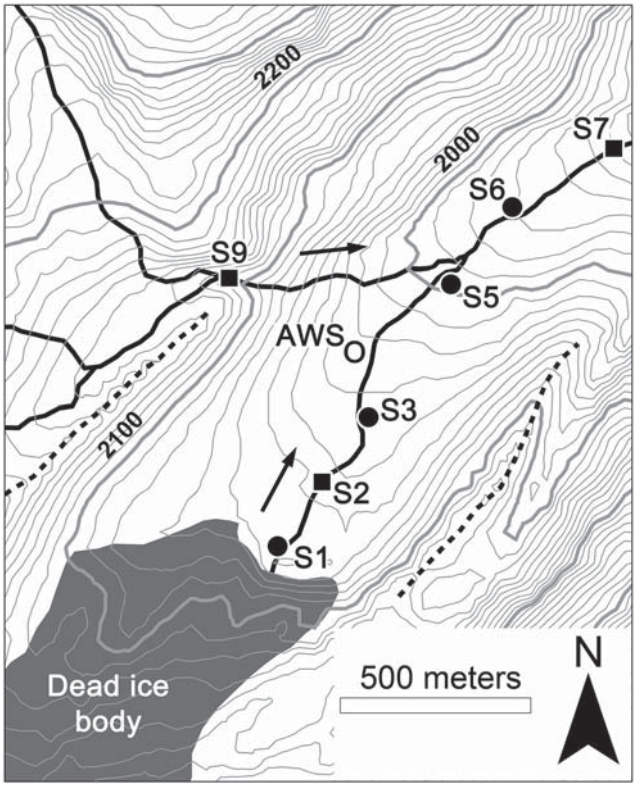

Figure 1. The Damma glacier forefield: lateral moraines are indicated with dashed black lines. At sites S1, S3, S5 and S6 (solid circles), stream and groundwater levels are recorded. At sites S2, S7 and S9 (solid squares), only stream stage is measured. An automatic weather station (AWS) is located in the middle of the forefield. Terrain elevation is shown by 10-m contour intervals. (Figure adapted from Magnusson *et al*., 2012a,2012b)

STUDY SITE

The study area, the Damma glacier forefield (Figure 1), is part of a small (10.7 km^2) granitic catchment situated in the central Swiss Alps. The glacier covers 40% of the catchment area and has been retreating since the end of the Little Ice Age (LIA). Large lateral moraines date from approximately 1850 (the end of the LIA) and two terminal moraine bands dating from 1927 and 1992 mark the end of two short periods of re-advance. The catchment ranges from 1792 to 3630 m a.s.l. and is snow-covered for approximately 6 months per year. The forefield spreads from roughly 1900 to 2100 m a.s.l. and covers an area of approximately 0.5 km^2. The site is inaccessible by road and heavy equipment can only be transported by helicopter. Those conditions limited our experimental possibilities, but they are typical constraints encountered in alpine sites.

On the basis of 3 years of data, the mean annual air temperature at the forefield is 2.2 °C; mean annual precipitation and mean annual runoff for the whole catchment are approximately 2300 and 2700 mm, respectively (Hindshaw *et al*., 2011). Evapotranspiration constitutes a small part of the water balance and was estimated to be 70 mm in 2008 (Kormann, 2009). The positive water balance is due to the negative mass balance of the glacier. Overall, the hydrology of the forefield is highly dominated by glacier and snow melt, creating strong daily and seasonal fluctuations in stream flow and, naturally, stream stage.

Magnusson *et al*. (2012a) studied four groundwater transects (named S1, S3, S5 and S6 in Figure 1). Each transect was equipped with three pressure transducers each: one in the stream and two in groundwater tubes placed on a line perpendicular to the stream. In this paper, we focus on site S3 (Figure 2), which was further equipped with the circular array of boreholes detailed in the Methods Section. In the manuscript, we refer to each tube of the initial S3 transect as $S3_{stream}$ for the stream stage measurement, $S3_{near}$ for the groundwater tube that is closest to the stream and $S3_{far}$ for the farthest from the stream. Groundwater levels at S3 suggest infiltration from the stream and display pronounced diurnal fluctuations during glacier ablation. S3 was chosen for this study because it presented some of the best soil conditions in the forefield for ERT, as well as a hydrogeological context representative of a large central part of the forefield.

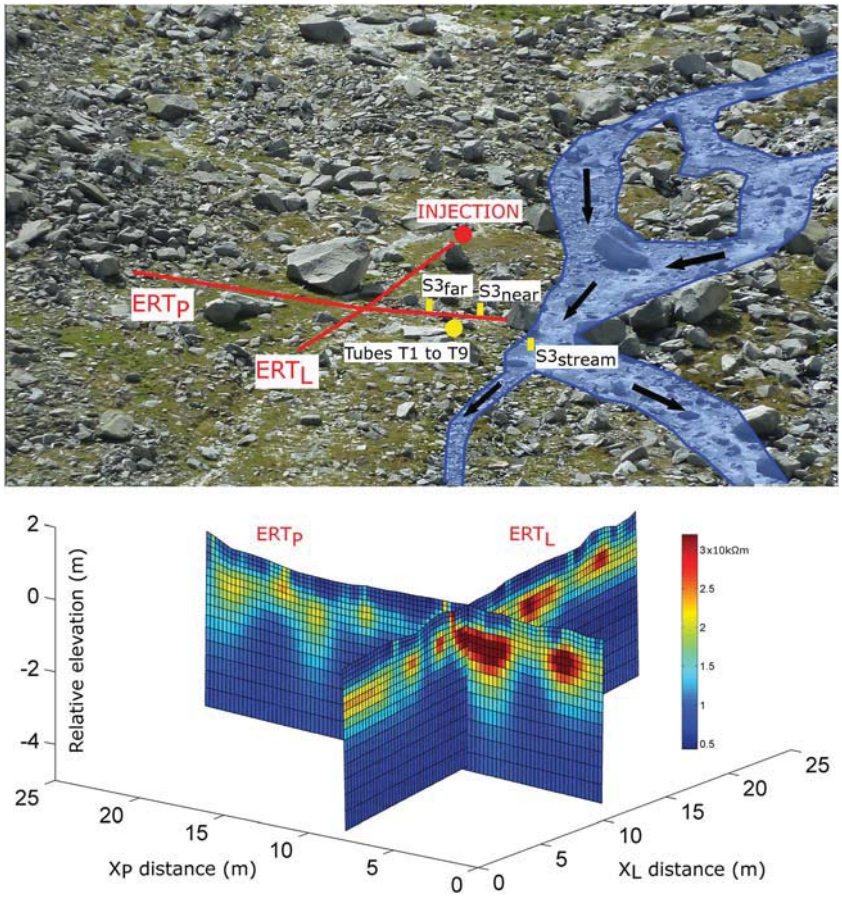

Figure 2. Layout of the longitudinal electrical resistivity tomography (ERT_L) and perpendicular ERT (ERT_P) lines at S3. The stream is highlighted in blue. In yellow are the S3 transect (rectangles) and groundwater tubes T1 to T9 (circle, see Figure 6 for details). The tomograms show background resistivity before salt injection. The lines cross at $X_L = 10$ m and $X_P = 8$ m. The resistivity colour scale is expressed in kΩ m

The installation of the groundwater tubes allowed documenting the layered structure of the subsurface. The top layer was approximately 20 cm thick and consisted of moist silts with shallow grass roots. The silty surface had a low permeability as witnessed by surface scour from summer storms. The next layer between 20- and 80-cm depth was a dry and poorly sorted mixture of sand, gravel, cobbles and occasionally large boulders. Below this layer, the number of boulders decreased and the saturated zone was reached at about 100-cm depth. We expect this layering to be typical of the flatter area of the forefield surrounding S3 (flood-plain type). Geophysical experiments (ERT and seismic) of a larger scale than those presented here (200 m long, 30- to 40-m penetration depth) have not shown a shallow bedrock boundary. The depth of moraine sediments appeared to exceed 10 m in most of the forefield, with a likely depth to bedrock of more than 20 m at S3. The hydrogeological context at S3 is therefore deeper than monitored by our ERT experiments, which only penetrated to 4.5-m depth. The limited depth of investigation is a trade-off for a higher spatial resolution.

METHODS

Inter-borehole experiments

A circle of eight groundwater tubes around a ninth central tube (see Figure 6 for a schematic diagram) was installed using the same method as for the initial S3 transect (Magnusson *et al.*, 2012a). The circle is approximately 1 m in diameter, where the central tube is located to form an equilateral triangle with $S3_{far}$ and $S3_{near}$ (Figures 2 and 7).

In addition to those already installed at $S3_{near}$, $S3_{far}$ and $S3_{stream}$, we installed pressure sensors (HOBO U20 Water Level Logger) in five of the new groundwater tubes (T2, T3, T5, T8 and T9) to follow the evolution of the water table gradients. This was carried out following the same methods as those of Magnusson *et al.* (2012a). The gradient of the groundwater table was calculated, interpolating data from the five tubes of the circle where the pressure sensors were installed.

For the salt tracer experiments, the electrical conductivity (EC) sensor WQ-Cond-1 was used with the Global Water GL500 data logger (measurement range

0–200 µS/cm with a precision of ±0.5%). Temperature was also recorded with a precision of ±0.2 °C. A hand-held device was used (WTW Cond 315i, with a precision of ±0.5%) for electrical conductivities higher than 200 µS/cm. At the start of each experiment, a saline solution at 1000 µS/cm was injected in T9 and the resulting changes in EC were continuously recorded in the surrounding tubes to determine the time of arrival of the tracer. We did not correct the resistivity values for temperature as the water temperature stayed constant during the experiment.

ERT measurements

Data acquisition and processing methods. In this section, we present specific details regarding acquisition, processing and quality control of the geophysical data. We built an ERT line consisting of two non-reversible lines with 48 electrodes. As illustrated in Figure 2, we installed the ERT lines in a cross pattern. The electrode spacing was 0.5 m for both lines. In the following, we will refer to the longitudinal line as ERT_L (parallel to the river) and to the perpendicular line as ERT_P (orthogonal to the river). The lines cross at the 17th electrode of ERT_P ($X_P = 8$ m) and the 21st electrode of ERT_L ($X_L = 10$ m). Both lines are numbered conventionally, starting at the downstream end of the line for ERT_L and the stream shore for ERT_P.

Data were acquired with a SYSCAL Pro Switch from Iris Instruments. Each measurement was stacked three to six times with an acquisition time of 250 ms. Measurement tests were conducted using Wenner, Wenner–Schlumberger and Dipole–Dipole configurations, the latter being typically used to carry out salt tracer tests (Kemna *et al*., 2002). In our case, however, the noise content of the Dipole–Dipole configuration was too high, and the Wenner–Schlumberger configuration showed the best results. We used 23 levels with the latter array to reach a maximum depth of investigation of 4.5 m. Resolution could have been further improved by adding intermediate levels; this would, however, have been too time-consuming for minimal gain.

The galvanic contact of the electrodes of both ERT_L and ERT_P with the ground was of good and constant quality. ERT_L showed the smallest contact resistances, with most electrodes in the 20–30 kΩ range, all being below 50 kΩ. The highest values (40–50 kΩ) were found in the vicinity of the lines' crossing area (electrodes 18–24). ERT_P was slightly poorer, with contact resistances mostly in the 30- to 40-kΩ range and some up to 80 kΩ. The area where the lines cross is degraded with local surface scour, resulting in more sand and boulders and less silt. The electrodes in the vicinity of this crossing point were in the 40- to 50-kΩ range for both lines.

The time-lapse inversion, i.e. the inversion of several ERT measurements conducted at different times along the same survey line, was carried out with the inversion software RES2DINV (Loke, 2006). The 'robust smoothness' constraint was used as a time-lapse inversion constraint (Claerbout and Muir, 1973), which minimizes the absolute changes in model resistivity values. The inversion was conducted sequentially, meaning each time step is inverted after the previous, and we based the reference model on the first data set (background state). A time-lapse damping factor of 0.5 was used to give priority to each model's smoothness rather than minimizing the changes between each time step (Loke *et al*., 2003). The site topography is reasonably smooth along ERT_P and ERT_L. It was surveyed every 1 m and included into the model with a damped distortion of the finite element grid.

We tested various methods to filter raw data of the ERT measurements (i.e. Hilbich *et al*., 2011; Rosset *et al*., 2013). For time-lapse studies, it is preferable that the same data points are removed from all data sets, even if erroneous data occur only at one time instance. We found that removing potentially erroneous data points did improve neither the mean absolute error of the inversion model nor the geometrical properties of the tomogram (for the intended use in this paper). Also, the small amount of noise present in our Wenner–Schlumberger surveys was rather random than systematic, making it difficult to eliminate the same data points for every survey. The inversion of both background conditions and the subsequent tracer test measurements was therefore completed with the raw data and resulted in mean absolute errors of less than 3%, which is a generally acceptable value for geo-electrical inversion.

Defining background conditions for time-lapse ERT. Figure 2 shows the experimental setup and the background ERT measurements. Note that the depicted tomograms include the lower corners, which have higher uncertainty than the rest of the tomogram. The three layers (conductive, resistive, conductive) witnessed during the installation of the groundwater tubes are clearly visible. Successive zones of high resistivity contrasts indicate the transitions between each layer. The thickness of the first two layers is slightly larger than observed during the installation of the tubes (Study Site Section). This is partly due to the diffusive nature of the geo-electrical method. It is also accentuated by the high conductivity contrasts between the three layers of the underground. At $X_P = 5$ m, we can notice that a probable subsurface boulder alters the modelled resistivity at least 1 m below it.

Salt tracer injection. Given the low permeability of the silty surface layer, we dug a 75-cm deep hole approximately 1.5 m upstream of the uppermost electrode (at $X_L = 25$ m), into which we injected a saline solution for ERT time-lapse monitoring. On 19 October 2012, we injected 3 kg of salt diluted in approximately 15 liters of

stream water. After 15 min, the solution had infiltrated. We consider this injection as a 'point' injection when compared with the temporal and spatial scales of the experiment. During the tracer experiment, the ground was snow-covered (5–20 cm deep). Both days had surface freeze in the morning and light snowmelt in the afternoon. Given the low permeability of the silty surface layer and the continuous snow cover, we consider that the surface temperature and moisture content did not vary significantly to cause surface resistivity changes. Because of these conditions, we could not specifically improve electrode contacts of the poorer electrodes by wetting. Note that the high salt concentration led to slow sinking of the plume because of density effects (Figures 3 and 4). This does, however, not affect our analysis in terms of advection velocity as we only follow the horizontal component of the plume's centre of mass.

Radon measurements

Under specific assumptions discussed later, the radioactive noble gas radon (^{222}Rn, half-life 3.82 days) can be used to estimate the residence time of young groundwater. When nearly radon-free stream or melt water infiltrates into the aquifer, it gradually becomes enriched with radon, generated by the decay of radium (^{226}Ra) present in the aquifer material. If no gas transfer occurs in the groundwater, the radon concentration increases with time. After about four half-lives (~15 days), the radon concentration in the groundwater reaches steady state as the decay rate comes into equilibrium with the production rate. Hence, if the equilibrium concentration is known, measurements of the radon concentration in groundwater give an estimate of the time that has passed since the water was last in contact with the atmosphere, which is the residence time of groundwater in the aquifer (Hoehn and von Gunten, 1989).

In 2010 and 2012, we collected 31 groundwater samples from various locations in the forefield, including all groundwater transects. Before sampling, the tubes were flushed twice with a bailer to remove stagnant water. For each sample, as in the work of Hoehn and von Gunten (1989), a small submersible pump was used to fill a narrow-necked 250-ml glass bottle until overflow. These sampling precautions reduce losses of radon by outgassing and are required for reproducible and relevant results. Each groundwater sample was analysed four times to provide an average radon concentration. Similar to Vogt *et al*. (2010), we used a Rad7-radon detector (Durridge Co.) to measure ^{222}Rn in 250-ml samples (Magnusson *et al*., 2012a). Some of the radon measurements were analysed on site with a portable instrument. The remaining samples were transported to the laboratory, and the results were corrected for decay during this time interval.

The highest concentration measured in the forefield was 106.4 Bq/l, with several measurements above 95 Bq/l (Magnusson *et al*., 2012a). We assume that this maximum concentration corresponds to the endmember in the forefield. There are two underlying assumptions: (1) our endmember value was measured from water that has reached steady-state conditions and (2) the local mineralogy and soil properties result in a constant and uniform rate of radon production across the forefield. The first assumption is fair given that 31 samples were collected at various locations across the forefield, including wells far away from the stream. The

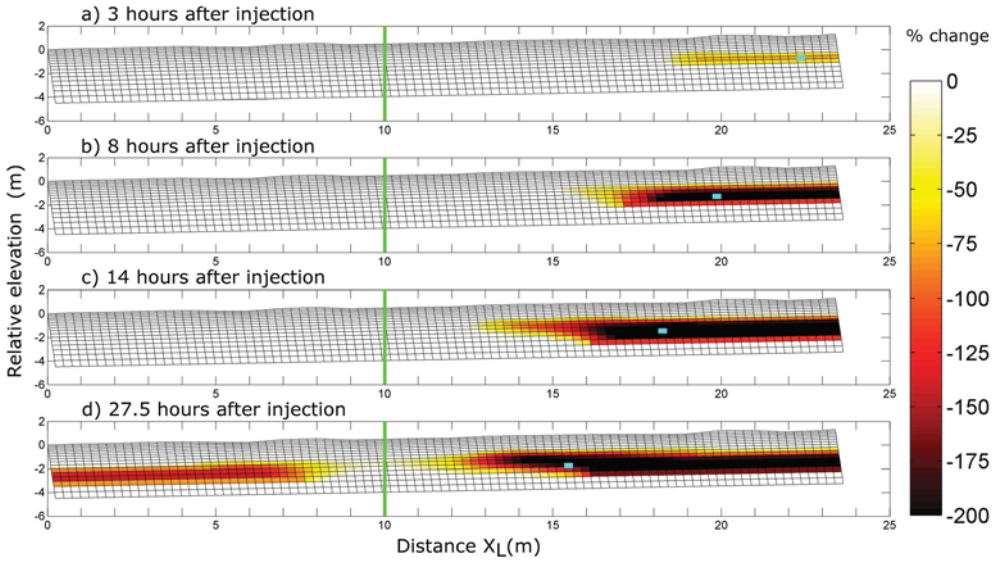

Figure 3. Successive measurements at longitudinal electrical resistivity tomography (ERT_L) during the tracer experiment. Results are expressed in percentage resistivity change from the background tomogram ($[R - R_0]/R_0 \times 100$) shown in Figure 2. The light blue rectangles represent the centre of mass of the plume along ERT_L. The green line indicates the crossing point with perpendicular ERT (ERT_P)

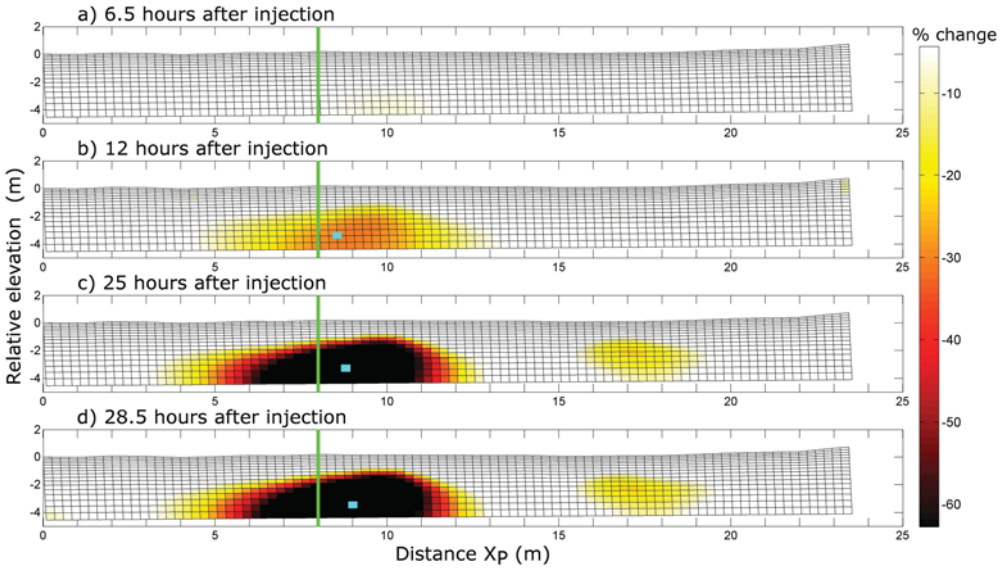

Figure 4. Successive measurements at perpendicular electrical resistivity tomography (ERT_P) during the tracer experiment. Results are expressed in percentage resistivity change ($[R - R_0]/R_0 \times 100$) from the background tomogram (Figure 2). The light blue rectangles represent the centre of mass of the plume along ERT_P. The green line indicates the crossing point with longitudinal electrical resistivity tomography (ERT_L). Note that the colour scale is different from Figure 3

second assumption is motivated by work from Bernasconi and the BigLink consortium (2011) and Smittenberg *et al.* (2012), who demonstrated that the entire Damma glacier catchment is located in the same granite body and the soils only shows small mineralogical variations.

RESULTS

Geophysical imaging of the salt plume

Longitudinal ERT line. Figure 3 shows successive ERT_L measurements during the tracer test. They allow the determination of both groundwater advection velocities and the groundwater flow direction. As described in the Methods Section, the injection point is located at $X_L = 25$ m, 1.5 m directly upstream of the ERT_L line. Spatial moments (Singha and Gorelick, 2005) were calculated for each time step to estimate the plume's centre of mass and thus its median advection velocity.

Figure 3a presents ERT_L 3 h after the start of the tracer test. By that time, some tracer has travelled 6.75 m. This first arrival represents preferential flow paths at a velocity of 54 m/day. In Figure 3a, the centre of mass of the plume has travelled 2.7 m (21.8 m/day). For the following three measurements, the centre of mass is, respectively, 5.2, 6.7 and 9.5 m away from the injection point, which corresponds to advection velocities of between 8.3 and 15.5 m/day. The plume spreads significantly over time, covering the whole investigation length after 27.5 h (Figure 3d).

Perpendicular ERT line. The ERT_P line provides important additional information on the direction of the groundwater flow (Figure 4). Note that the colour scales in Figures 3 and 4 are not identical. The ERT lines cross at $X_P = 8$ m for ERT_P and $X_L = 10$ m for ERT_L. Spatial moments show that the plume is centred at $X_P = 9$ m at the end of the experiment (blue rectangle in Figure 4d). This corresponds to a median deviation of the salt plume from the direction of the ERT_L line of 3.8°. This confirms previous results that had evidenced this location as a losing reach and provides a reliable direction for groundwater flow. Advection velocities inferred from ERT_L are justified as they were determined using a cross-section appropriately parallel with the flow direction.

The ERT_P line provides additional information on the velocity of the fastest groundwater flow paths. Figure 4a shows first signs of tracer crossing the perpendicular line, which corresponds to a tracer velocity of 55.4 m/day. Although this result is in line with the corresponding estimate from ERT_L, this velocity is potentially over-estimated because of the three-dimensional nature of the ERT method. The electrical field created by ERT_P is a half sphere, and some tracer along the ERT_L line will be detected before it actually crosses the ERT_P transect. We did not calculate median advection velocities from ERT_P, as this would have required using temporal moments. Calculating temporal moments would be suited for a longer time series with preferably a higher temporal resolution.

Note that the resistivity changes at the crossing point between ERT_L and ERT_P show small differences. The conductivity changes in ERT_L are somewhat weaker than those witnessed at $X_P = 8$ m in ERT_P. This may originate from the independent smoothing of both inversion models

(Hauck *et al.*, 2003). Also, as both lines are perpendicular to each other, the asymmetrical electrical fields created by both lines at the crossing point will be different, resulting in locally inconsistent resistivity estimates.

Circular borehole array

Salt tracer experiments. On several occasions, we injected salt solutions into the centre tube T9 and measured the subsequent EC changes in the surrounding tubes (see Figure 6 for a schematic of the borehole array). A rise in EC was detected in T3 and T4 after each injection, whereas T5 was only reached in one of the experiments. Figure 5 presents the EC changes measured in T3 and T4, following an injection in tube T9 at 19:35 on 27 August 2013. The EC in T9 is not depicted as it remained above 200 µS/cm over the duration of the experiment. Similar to the analysis of the ERT data, the median travel time of the salt plume was calculated for each tube. Median advection velocities were 5.7 m/day to T3 and 11.2 m/day to T4. In the discussion, we show that these results provide hydraulic conductivity values that are consistent with the results of the ERT tracer test.

Groundwater gradient analysis. Figure 6 shows alpha (α), the angle between the ERT_L downstream direction (blue arrow) and the groundwater flow direction (thick black arrow). Alpha is positive for groundwater flow away from the stream. Using groundwater level in five tubes, we fitted a plane representing the surface of the saturated zone. From this plane, the slope of the groundwater table and alpha was inferred. Alpha varied slightly over the duration of our observations, but no distinct seasonal or diurnal variations could be found. The median alpha value was 17.2°. Averaged over the duration of the salt tracer experiment illustrated in Figure 5, the groundwater gradients were 2.2% between T9 and T3, and 5.0% between T9 and T5.

Radon measurements

We measured radon concentrations on three separate occasions at S3 (Table I) and other transects in the forefield. In total, 31 samples were analysed. At S3, the concentrations varied during the season, but $S3_{far}$ always had higher radon concentrations than $S3_{near}$, confirming that groundwater is recharged along this reach. However, radon concentrations at S3far were low compared with measurements at the other transects. Under the assumptions outlined in the Methods Section, the concentrations measured at S3 indicate residence times varying between 0.4 and 1 days. In the discussion, we will compare the average estimated groundwater age at $S3_{far}$ (0.72 day in 2012) against potential travel times to $S3_{far}$ using the experimental range of flow directions and advection velocities.

DISCUSSION

Groundwater flow properties

Table II presents a summary of the estimated groundwater advection velocities using results from ERT_L and inter-borehole experiments. From Figure 3d, we can infer that the groundwater table follows the surface topography, which has an average gradient of 5.6% along the ERT_L line. Because the flow is almost parallel to the stream, we assume that the hydraulic gradient is equal to the longitudinal gradient. On the basis of this gradient and a porosity value of 0.3 (Smittenberg *et al.*, 2012, at their site 11), hydraulic conductivities were calculated by inverting Darcy's law (Table II). Hydraulic conductivities resulting from the inter-borehole tracer experiments were calculated using

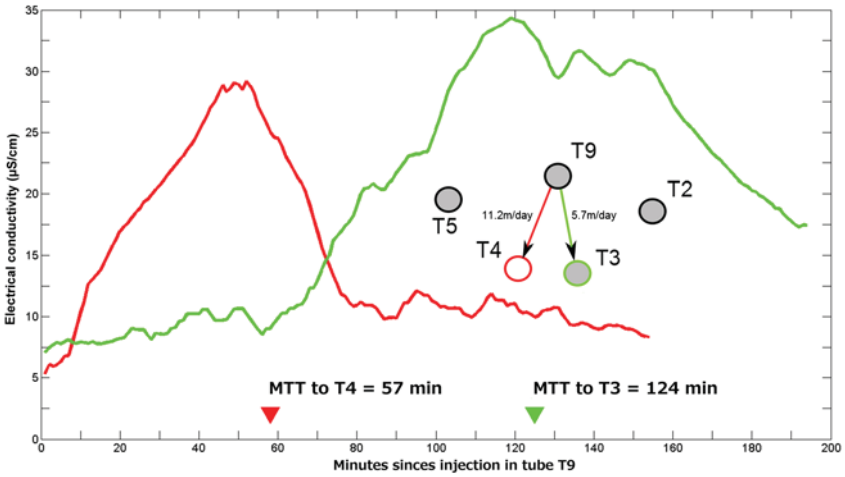

Figure 5. Results of a salt injection into T9 at 19:35 on 27 August 2013. Electrical conductivity is plotted at T3 (green) and T4 (red) as a function of time since injection. Red and green triangles indicate the median transit time (MTT) to T3 and T4, respectively

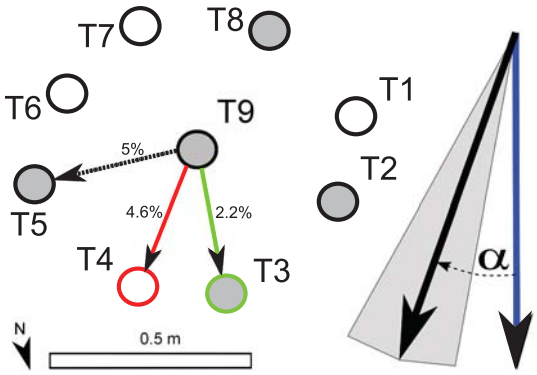

Figure 6. Schematic of the borehole array. The tubes filled in grey were equipped with pressure sensors. Groundwater gradients from T9 to T3 and from T9 to T5 were measured. The gradient to T4 is an interpolation. Alpha (α) is the angle between the electrical resistivity tomography line downstream direction (blue arrow) and the gradient of the groundwater table (thick black arrow). The variability of alpha is illustrated by the grey area

the local hydraulic gradients of 2.2% to T3 and 5% to T5 (Figure 6). In addition, we assume that the groundwater table is a plane intersecting the measured groundwater levels at T3, T5 and T9. This plane yields a gradient of 4.6% for the direction from T9 to T4.

Advection velocities ranged, respectively, from 8.3 to 21.8 m/day with ERT_L, resulting in hydraulic conductivity estimates varying between 0.51×10^{-3} and 1.35×10^{-3} m/s. The inter-borehole experiments resulted in advection velocities varying between 5.7 and 11.2 m/day. Because the hydraulic gradient was lower within the inter-borehole array, the calculated hydraulic conductivity ranged from 0.86×10^{-3} to 0.90×10^{-3} m/s. Averaging at 0.88×10^{-3} m/s, the local hydraulic conductivity estimates are high but realistic given the grain size distribution (mainly sand and gravel) observed during the installation of the groundwater tubes (David Carrier, 2003; Song *et al.*, 2009). All experimental values are consistent, despite covering spatial scales varying from 0.5 to 25 m. This is a remarkable achievement considering the experimental difficulties involved and the apparent heterogeneity of the soils.

Those results are roughly an order of magnitude greater than hydraulic conductivity estimates from earlier slug tests at $S3_{near}$ and $S3_{far}$ (Magnusson *et al.*, 2012a), which varied between 0.3×10^{-4} and 1.3×10^{-4} m/s, averaging at 0.6×10^{-4} m/s. However, as groundwater levels during slug tests were low, they were carried out by injecting water into the boreholes. This may have led to the estimation of partly unsaturated hydraulic conductivity, which could be several orders of magnitude lower than saturated hydraulic conductivity. Slug tests are also less spatially integrated than the methods presented here. They are therefore likely to provide estimates, which are more subject to local heterogeneities.

Regarding the direction of the groundwater flow, the losing character of the reach was confirmed by both methods, although the ERT analysis yielded a flatter angle (3.8°) than the borehole array (17.2°). This could be due to the closer proximity to the stream of the groundwater tubes than the ERT_L line (c.f. discussion that follows).

Conceptual model of the stream reach

Before this study, it was essentially unknown whether groundwater at this transect was originating from the lateral moraine to the east (Figure 1) or from the stream, and at which distance it had infiltrated into the aquifer. On the basis of the groundwater flow direction yielded from ERT and inter-borehole experiments, we can hypothesize that groundwater infiltrates from the stream. The short residence times at $S3_{near}$ and $S3_{far}$ estimated from radon measurements indicate that infiltration from the stream into the aquifer must happen within a close range of the S3 transect. A sharper angle away from the stream was also witnessed at the borehole array, which suggests that flow paths may curve close to the stream, such as similarly identified by Rodhe and Seibert (2011) for a gaining reach.

In Figure 7, we deploy a simplified geometry to verify these hypotheses. We focus on $S3_{far}$ as $S3_{near}$ is apparently very close to its infiltration zone. Using groundwater flow direction ranging from 3.8 to 17.2° (Figure 7, dashed red lines), we yield potential flow paths to $S3_{far}$ varying from 10 to 25 m (Figure 7, lighter blue stream area).

Table I. Radon concentration measurements and corresponding estimated age of groundwater at the S3 transect

Location	$S3_{near}$			$S3_{far}$		
	Concentration (Bq/L)	Standard deviation (Bq/L)	Age (days)	Concentration (Bq/L)	Standard deviation (Bq/L)	Age (days)
19 July 2010	8.5	1.8	0.44	12.0	1.5	0.64
6 September 2010	11.5	2.0	0.61	17.4	1.0	0.96
15 August 2012 10:20	8.2	0.8	0.42	12.9	2.5	0.69
15 August 2012 13:00	9.5	0.7	0.49	13.7	2.8	0.74
15 August 2012 16:10	8.6	1.8	0.44	13.8	2.8	0.74

Table II. Minimum and maximum hydraulic conductivities (10^{-3} m/s) calculated using estimated advection velocities (m/day) and hydraulic gradients (%)

Method		ERT_L	Tube T9 to T3	Tube T9 to T4
Advection velocity (m/day)	Min	8.3(3d)	5.7(5)	—
	Max	21.8(3a)	—	11.2(5)
Hydraulic gradient (%)		5.6%(3d)	2.2%(6)	4.6%(6)
Hydraulic conductivity (10^{-3} m/s)	Min	0.51	0.86	—
	Max	1.35	—	0.90

Exponents indicate which figure and subplot are used to calculate advection velocities and hydraulic gradients.
ERT_L, longitudinal electrical resistivity tomography.

Such a range of flow path lengths combined with the experimental range of advection velocities (5.7–21.8 m/day as per Table II) lead to mean travel times to $S3_{far}$ varying from 0.46 to 4.39 days. According to the radon measurements, the groundwater age at $S3_{far}$ was 0.72 day, which could for instance originate from a 10-m-long flow path at 13.9 m/day. This example shows that the hypothesized flow paths (Figure 7, dashed blue lines) are realistic and that radon age estimates suggest rather short and fast flow paths (Figure 7, thick dashed blue line). This means that the discrete solute plumes may have travelled slightly slower than the median pore water velocity. A similar result was presented by Rovey and Niemann (2005), who showed that the advection velocity of solute plumes in a heterogeneous medium can be significantly slower than the average pore water velocity.

The combination of directional information, groundwater age estimates and advection velocities allowed us to better understand the two-dimensional aspects of groundwater flow in the vicinity of the investigated stream reach. We conclude that groundwater flow to $S3_{near}$ and $S3_{far}$ does not originate from high up in the moraine, but from the nearby streambed. Flow paths are potentially shorter and faster than ERT results suggested alone (Figure 7, dashed red line with direction 3.8°).

Methodological perspectives

From a methodological standpoint, the borehole array provided good independent second estimates of both hydraulic conductivity and direction of the groundwater flow. Although it did not provide qualitatively different information than the orthogonal pair of ERT lines, it provided data representative of a smaller scale. A combination of both approaches is certainly beneficial given the uncertainties inherent to each of the methods. We therefore consider that all experiments deployed in this study added value and complemented each other.

Should invasive techniques not be implementable, the ERT setup would suffice to obtain a first understanding of the site. The ERT experiment is also easier to implement at other stream reaches than the borehole array. The circular setup of ground water tubes may, however, be more suitable if flow direction changes over small distances or if the

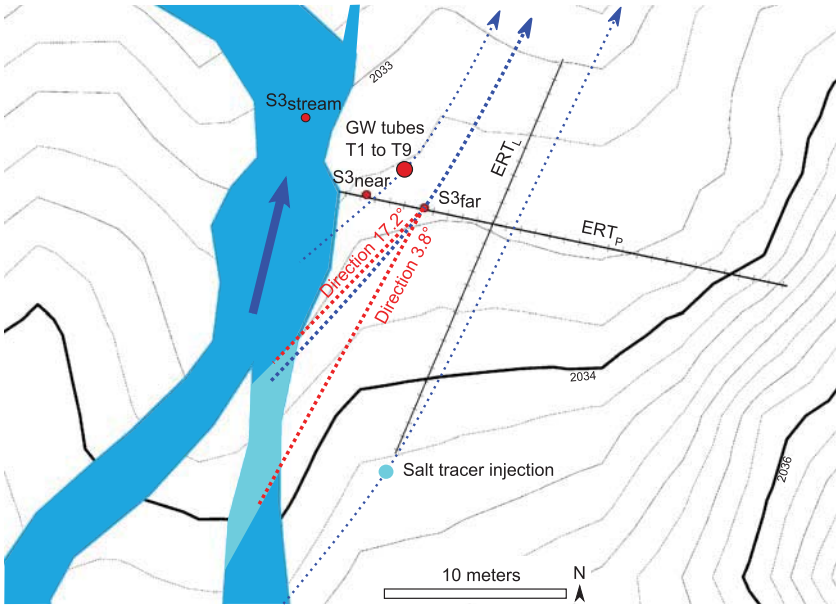

Figure 7. Sketch of the experimental setup and conceptual interpretation of the results (see Figure 2 for a photograph). The dashed red lines constrain the lighter blue infiltration area to $S3_{far}$ with the directional results of both the electrical resistivity tomography (ERT) setup and the borehole array (T1 to T9). Hypothesized flow paths through $S3_{far}$, through the ERT setup and through the borehole array are indicated as dashed blue arrows

subsurface flow regime shows diurnal variations. Such situations could be hard to resolve by ERT experiments. Using colour tracers is also possible for the borehole array, should the use of salt as a tracer be prohibited.

The strength of this study was to overcome experimental difficulties by combining different methods. This enabled us to confidently estimate groundwater flow properties and develop a conceptual model of groundwater and stream water interactions at a particular stream reach. This research field has recently seen intense efforts, including an increasing number of interdisciplinary case studies; see Krause *et al.* (2014) for an overview of significant recent articles. Langston *et al.* (2013) combined heat and solute tracer analyses in a pro-glacial moraine of the Canadian Rockies. Their hydraulic conductivity estimates varied between 0.3 and 3×10^{-3} m/s, which is very similar to our experimental range. Complementary numerical modelling of flow and solute transport during tracer experiments (i.e. Dafflon *et al.*, 2011) can also help reducing the uncertainty in the estimation of hydrological parameters and their spatial distribution.

Krause *et al.* (2014) highlight the difficulty of transferring process understanding across spatial scales, a weakness of our present study. Despite conducting experiments that cover scales ranging from less than 1 to 25 m, we would still need additional work to extend our findings to the entire forefield. Binley *et al.* (2013) for instance used electromagnetic induction to continuously measure stream water EC along a river bed, in addition to combining various experimental methods. They witnessed strong spatial variability in groundwater flow directions whereas longitudinal changes in hydraulic conductivity were less apparent. This highlights the difficulty of balancing high sampling density with the aim of understanding hydraulic processes at the catchment scale. In steep alpine sites, measuring one physical parameter at a high spatial resolution tends to be difficult for experimental reasons. Using approaches that integrate over larger distances (Magnusson *et al.*, 2012b; Langston *et al.*, 2013) and multiplying the methods involved (Muir *et al.*, 2011) seem better avenues for both up-scaling purposes and confidently estimating local groundwater flow properties.

CONCLUSIONS

We carried out invasive and non-invasive experiments to determine the groundwater flow velocity and hydraulic conductivity near the stream flowing through the Damma glacier forefield. The non-invasive experiments consisted of two ERT_P lines. The invasive experiments involved installing a circular array of nine groundwater tubes, and then carrying out inter-borehole salt tracer experiments. We also monitored the two-dimensional gradient of the groundwater table within the circular array of boreholes via tubes equipped with pressure transducers.

Salt tracer tests monitored by ERT time-lapse experiments captured hydraulic conductivities from 0.51×10^{-3} to 1.35×10^{-3} m/s. The inter-borehole tracer experiments provided a narrower range of hydraulic conductivities. The mean value of 0.9×10^{-3} m/s is high but realistic for the coarse grained sediments witnessed during installation of the groundwater tubes. ERT analysis and groundwater level measurements also allowed inferring groundwater flow direction. Both not only confirmed that the stream recharges the aquifer at this reach but also showed that the flow is directed only slightly away from the stream. Radon measurements were used to estimate the age of groundwater at the transect, which helped confirm that the local groundwater flow originates from the streambed a short distance away rather than higher up the lateral moraine. Although the experimental methods presented in this study have potentially large uncertainties, which are individually difficult to assess, the consistency of groundwater flow direction and hydraulic conductivity estimates provides added confidence in those results.

The combination of directional information, groundwater age and advection velocities allowed us to extend our previous point-scale understanding of the groundwater properties at this transect to a two-dimensional conceptual model of the stream reach. This achievement is particularly noteworthy as subsurface conditions found on glacier forefields hamper typical investigation techniques and the heterogeneity of hydraulic properties makes point measurements unreliable.

ACKNOWLEDGEMENTS

Financial support for this study was provided by the SoilTrEC project of the European Union FP7. We thank SwissTopo for providing external data, which was essential to this study. The Soil and Terrestrial Environmental Physics (STEP) research group of the ETH Zürich kindly lent us the geophysical equipment required for this study. Clare Webster proofread the English. Andrew Binley and an anonymous reviewer provided comments that greatly improved the manuscript.

REFERENCES

Banwart S, Bernasconi SM, Bloem J, Blum W, Brandao M, Brantley S, Chabaux F, Duffy C, Kram P, Lair G, Lundin L, Nikolaidis N, Novak M, Panagos P, Ragnarsdottir KV, Reynolds B, Rousseva S, de Ruiter P, van Gaans P, van Riemsdijk W, White T, Zhang B. 2011. Soil processes and functions in Critical Zone Observatories: hypotheses and experimental design. *Vadose Zone Journal* **10**: 974–987. DOI:10.2136/vzj2010.0136.

Bernasconi SM, BigLink consortium. 2011. Chemical and biological gradients along the Damma glacier soil chronosequence, Switzerland. *Vadose Zone Journal* **10**: 867–883. DOI: 10.2136/vzj2010.0129.

Binley A, Cassiani G, Deiana R. 2010. Hydrogeophysics: opportunities and challenges. *Bollettino di Geofisica Teorica ed Applicata* **51**(4): 267–284.

Binley A, Ullah S, Heathwaite AL, Heppell C, Byrne P, Lansdown K, Trimmer M, Zhang H. 2013. Revealing the spatial variability of water fluxes at the groundwater-surface water interface. *Water Resources Research* **49**: 3978–3992. DOI:10.1002/wrcr.20214.

Claerbout JF, Muir F. 1973. Robust modeling with erratic data. *Geophysics* **38**: 826–844.

Dafflon B, Barrash W, Cardiff M, Johnson TC. 2011. Hydrological parameter estimations from a conservative tracer test with variable-density effects at the Boise Hydrogeophysical Research Site. *Water Resources Research* **47**: W12513. DOI:10.1029/2011WR010789.

David Carrier W. 2003. Goodbye, Hazen; hello, Kozeny-Carman. *Journal of Geotechnical and Geoenvironmental Engineering*. DOI: 10.1061/~ASCE!1090-0241~2003!129:11~1054!.

Garré S, Koestel J, Günther T, Javaux M, Vanderborght J, Vereecken H. 2010. Comparison of heterogeneous transport processes observed with electrical resistivity tomography in two soils. *Vadose Zone Journal* **9**: 336–349. DOI: 10.2136/vzj2009.0086.

Hauck C. 2002. Frozen ground monitoring using DC resistivity tomography. *Geophysical Research Letters* **29**(21): 2016. DOI: 10.1029/2002GL014995.

Hauck C, Vonder Mühll D, Maurer H. 2003. Using DC resistivity tomography to detect and characterize mountain permafrost. *Geophysical Prospecting* **51**: 273–284.

Hilbich C, Fuss C, Hauck C. 2011. Automated time-lapse ERT for improved process analysis and monitoring of frozen ground. *Permafrost and Periglacial Processes* **22**(4): 306–319. DOI: 10.1002/ppp.732.

Hindshaw RS, Tipper ET, Reynolds BC, Lemarchand E, Wiederhold JG, Magnusson J, Bernasconi SM, Kretzschmar R, Bourdon B. 2011. Hydrological control of stream water chemistry in a glacial catchment (Damma glacier, Switzerland). *Chemical Geology*. DOI: 10.1016/j.chemgeo.2011.04.012.

Hoehn E, von Gunten HR. 1989. Radon in groundwater – a tool to assess infiltration from surface waters to aquifers. *Water Resources Research* **25**: 1795–1803.

Kalbus E, Reinstorf F, Schirmer M. 2006. Measuring methods for groundwater – surface water interactions: a review. *Hydrology and Earth System Sciences* **10**: 873–887.

Kemna A, Vanderborght J, Kulessab B, Vereecken H. 2002. Imaging and characterisation of subsurface solute transport using electrical resistivity tomography (ERT) and equivalent transport models. *Journal of Hydrology* **267**: 125–146.

Kobierska F, Jonas T, Zappa M, Bavay M, Magnusson J, Bernasconi SM. 2013. Future runoff from a partly glacierized catchment: a two-model approach. *Advances in Water Resources* **55**: 204–214. DOI: 10.1016/j.advwatres.2012.07.024.

Kormann C. 2009. Untersuchungen des Wasserhaushaltes und der Abflussdynamik eines Gletschervorfeldes. Master's thesis. TU Dresden.

Krause S, Boano F, Cuthbert MO, Fleckenstein JH, Lewandowski J. 2014. Understanding process dynamics at aquifer-surface water interfaces: an introduction to the special section on new modeling approaches and novel experimental technologies. *Water Resources Research* **50**: 1–7. DOI:10.1002/2013WR014755.

Langston G, Hayashi M, Roy JW. 2013. Quantifying groundwater-surface water interactions in a proglacial moraine using heat and solute tracers. *Water Resources Research* **49**: 5411–5426. DOI:10.1002/wrcr.20372.

Loke MH, Acworth I, Dahlin T. 2003. A comparison of smooth and blocky inversion methods in 2D electrical imaging surveys. *Exploration Geophysics* **34**: 182–187.

Loke MH. 2006. RES2DINV ver. 3.55, Rapid 2D resistivity & IP inversion using the least-squares method. Software Manual; 139.

Magnusson J, Kobierska F, Huxol S, Hayashi M, Jonas T, Kirchner JW. 2012a. Melt water driven stream and groundwater stage fluctuations on a glacier forefield (Damma gletscher, Switzerland). *Hydrological Processes*. DOI: 10.1002/hyp.9633.

Magnusson J, Jonas T, Kirchner J. 2012b. Temperature dynamics of a proglacial stream: identifying dominant energy balance components and inferring spatially integrated hydraulic geometry. *Water Resources Research* **48**: W06510. DOI:10.1029/2011WR011378.

Miller CR, Routh PS, Brosten TR, McNamara JP. 2008. Application of time-lapse ERT imaging to watershed characterization. *Geophysics* **73**(3): 7–17. DOI: 10.1190/1.2907156.

Muir DL, Hayashi M, McClymont AF. 2011. Hydrological storage and transmission characteristics of an alpine talus. *Hydrological Processes*. DOI: 10.1002/hyp.8060.

Perri MT, Cassiani G, Gervasio I, Deiana R, Binley A. 2012. A saline tracer test monitored via both surface and cross-borehole electrical resistivity tomography: comparison of time-lapse results. *Journal of Applied Geophysics* **79**: 6–16. DOI: 10.1016/j.jappgeo.2011.12.011.

Rodhe A, Seibert J. 2011. Groundwater dynamics in a till hillslope: flow directions, gradients and delay. *Hydrological Processes* **25**: 1899–1909. DOI: 10.1002/hyp.7946.

Rovey CW, Niemann WL. 2005. Do conservative solutes migrate at average pore-water velocity. *Groundwater* **43**(1): 52–62. DOI: 10.1111/j.1745-6584.2005.tb02285.x.

Rosset E, Hilbich C, Schneider S, Hauck C. 2013. Automatic filtering of ERT monitoring data in mountain permafrost. *Near Surface Geophysics* **11**(4): 423–433. doi:10.3997/1873-0604.2013003.

Scherler M, Hauck C, Hoelzle M, Stähli M, Völksch I. 2012. Meltwater infiltration into the frozen active layer at an alpine permafrost site. *Permafrost and Periglacial Processes* **21**: 325–334. DOI: 10.1002/ppp.694.

Singha K, Gorelick SM. 2005. Saline tracer visualized with three-dimensional electrical resistivity tomography: field-scale spatial moment analysis. *Water Resources Research* **41**: W05023. DOI: 10.1029/2004WR003460.

Smittenberg RH, Gierga M, Goransson H, Christl I, Farinotti D, Bernasconi SM. 2012. Climate-sensitive ecosystem carbon dynamics along the soil chronosequence of the Damma glacier forefield, Switzerland. *Global Change Biology* **18**: 1941–1955. DOI: 10.1111/j.1365-2486.2012.02654.x.

Song J, Chen X, Cheng C, Wang D, Lackey S, Xu Z. 2009. Feasibility of grain-size analysis methods for determination of vertical hydraulic conductivity of streambeds. *Journal of Hydrology*. DOI: 10.1016/j.jhydrol.2009.06.043.

Vogt T, Hoehn E, Schneider P, Freund A, Schirmer M, Cirpka OA. 2010. Fluctuations of electrical conductivity as a natural tracer for bank filtration in a losing stream. *Advances in Water Resources* **33**(11): 1296–1308. doi:10.1016/j.advwatres.2010.02.007.

Ward AS, Gooseff MN, Singha K. 2010. Imaging hyporheic zone solute transport using electrical resistivity. *Hydrological Processes* **24**: 948–953. DOI: 10.1002/hyp.7672.